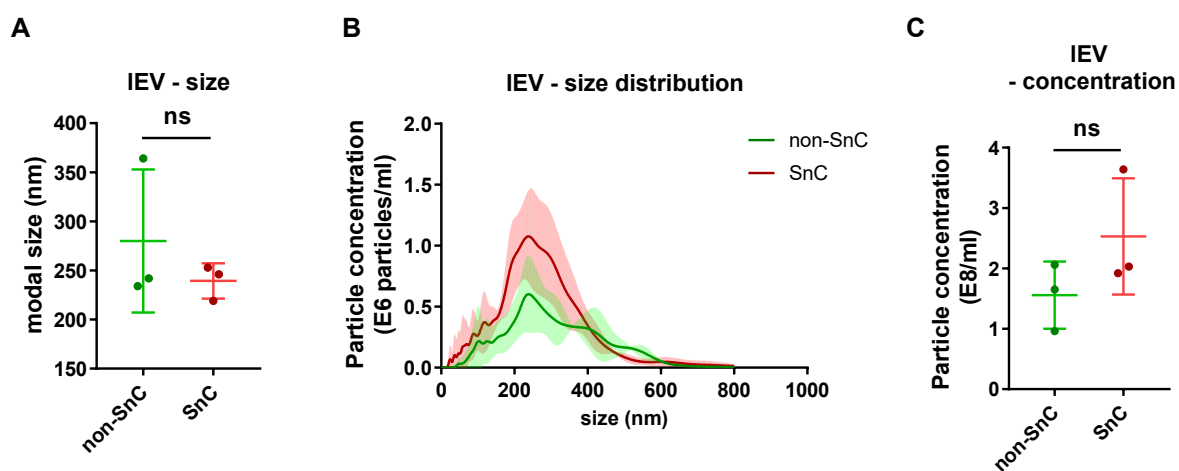**Supplementary Figures**



**Figure S1. Isolation and analysis of lEVs (microvesicles) from non-SnCs and SnCs by differential ultracentrifugation.** (A) NTA size measurements and (B) size distribution plot of lEVs derived from the same number of non-SnCs and SnCs (n = 3 per group). (C) NTA particle concentration measurements of non-SnCs and SnC-derived lEVs (n = 3 per group). All values are mean ± S.D. ns: not significant. A two-tailed unpaired t-test was used for statistical analysis.
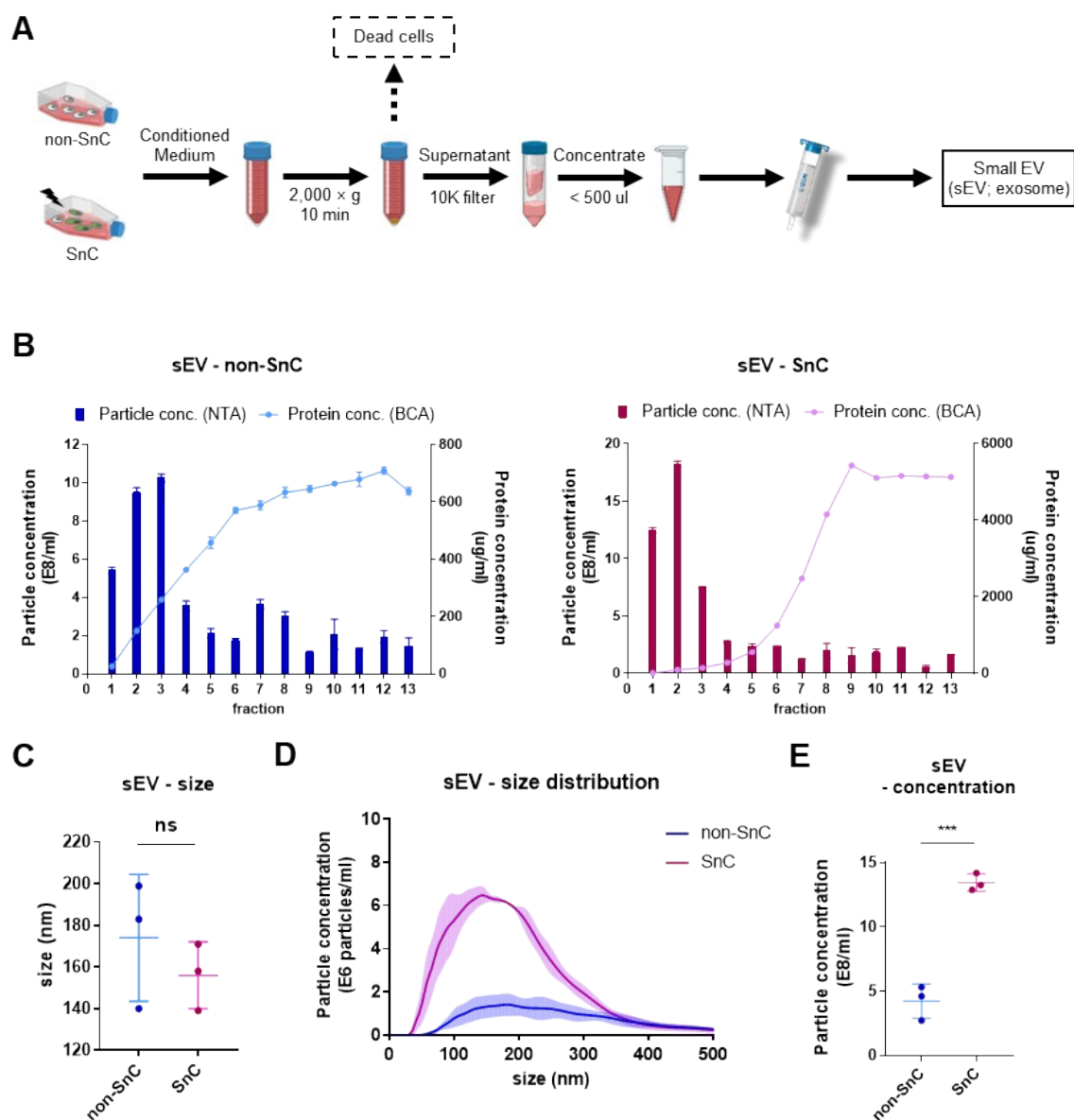
**Figure S2. Isolation and analysis of sEVs isolated from non-SnCs and SnCs by size exclusion chromatography (SEC).** (A) Schematic of the workflow for sEV isolation from non-SnCs or SnCs following the SEC method. (B) NTA particles and BCA protein concentration measurements of SEC fractions (1–13) from non-SnCs (left) and SnCs (right). (C) NTA size measurements and (D) size distribution plot of sEVs (fractions 1–3) derived from non-SnCs or SnCs cells (n = 3 per group). (E) NTA particle concentration measurements of sEVs (SEC fraction 1–3) (n = 3 per group). All values are mean ± S.D. ns: not significant, ***p < 0.001. A two-tailed unpaired t-test was used for statistical analysis.
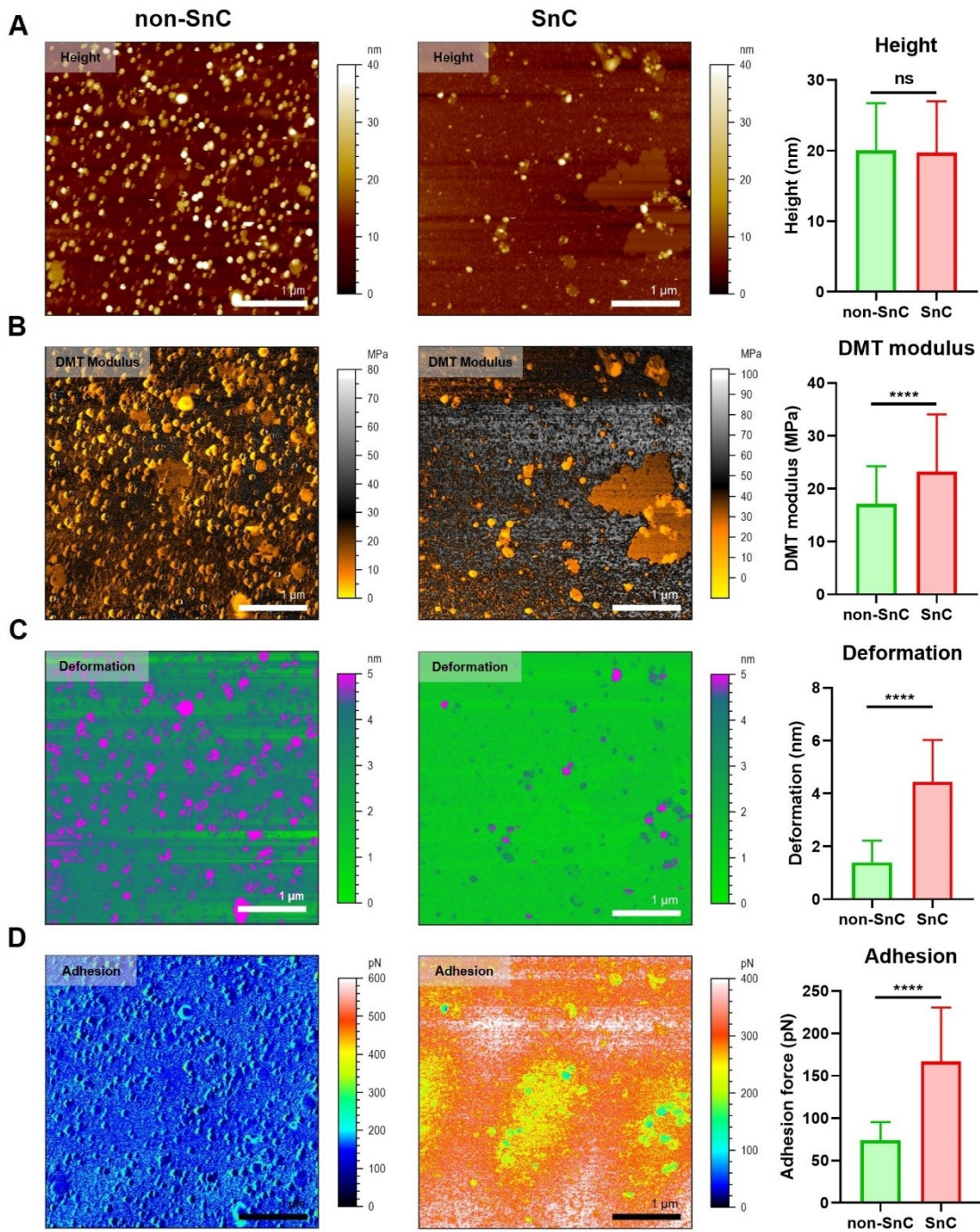
**Figure S3. Representative PF-QNM mapping of sEVs isolated from non-SnCs and SnCs**. (A) Topography (height), (B) DMT modulus (stiffness), (C) deformation, and (D) adhesion images and column bar graphs of each property. Scan size is 4 μm × 4 μm at 512 × 512 pixels. All values are mean ± S.D. ns: not significant, ***p < 0.0001. A two-tailed unpaired t-test was used for statistical analysis.
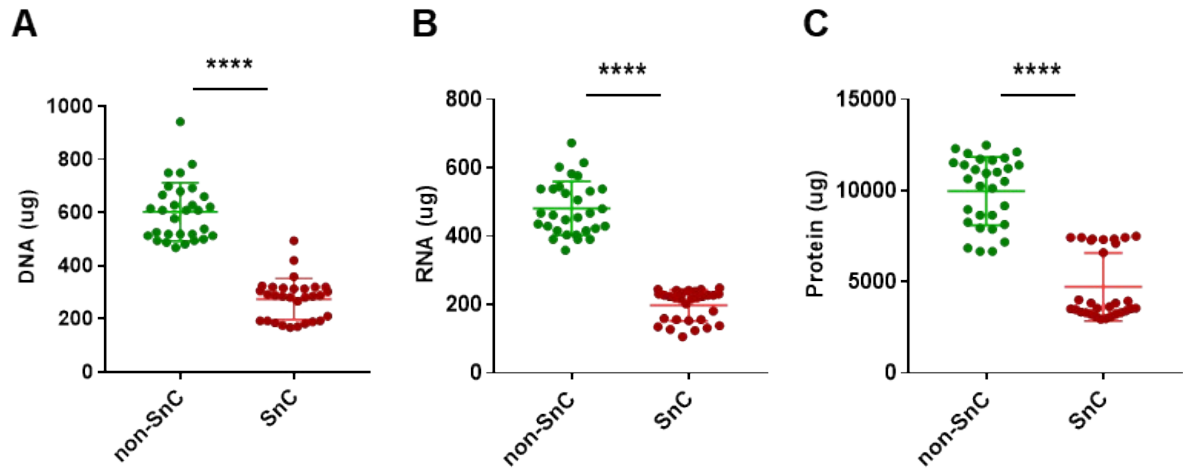
**Figure S4.** Quantification of the (A) DNA, (B) RNA, and (C) protein concentrations in non-SnC and SnC-derived sEV, normalized to the sEV concentration ($E^8$/mL) (n = 30 per group). All values are mean ± S.D. ****$p < 0.0001$. A two-tailed unpaired t-test was used for statistical analysis.
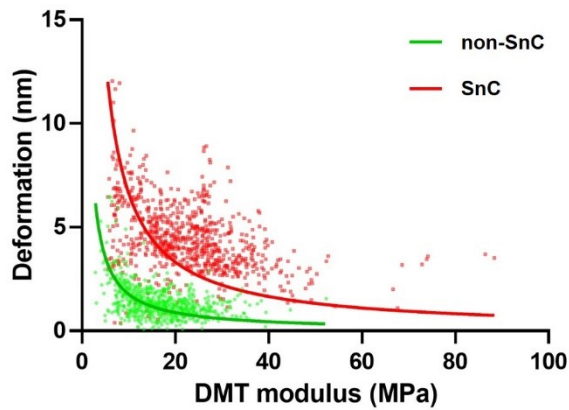
**Figure S5.** Mechanical property relationships of non-SnC and SnC-derived sEVs. The scatter plot (n = 800 for each condition) shows the relationship between deformation and the DMT modulus. Considering about 80 sEVs for each condition, the data acquisition was conducted by readout of 5~15 points per sEV (see MATERIALS AND METHODS for details). In both the non-SnC and SnC-derived sEVs, the deformation and DMT modulus values are inversely proportional at a constant scanning force (850 pN). This means that both types of sEVs follow the general Young's modulus definition. Interestingly, the overlap between the two datasets is small and the datasets seem to be separated from each other, indicating that the structure and composition of the sEVs have changed.[1] Recent results of PF-QNM analysis on multi-layered composites, including EVs, are similar to ours, supporting our interpretation.[2-5]
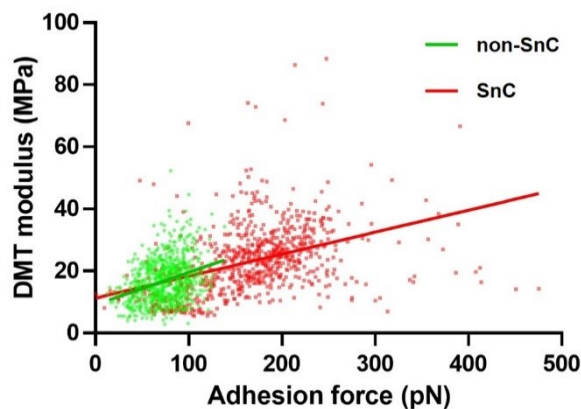
**Figure S6.** Mechanical property relationships of non-SnC and SnC-derived sEVs. The scatter plot shows the relationship between the DMT modulus and adhesion force. Considering about 80 sEVs for each condition, the data acquisition was conducted by readout of 5~15 points per sEV (see MATERIALS AND METHODS for details). In both the non-SnC and SnC-derived sEVs, the DMT modulus and adhesion force values are proportional. Specifically, although there is a proportional relationship between adhesion and the DMT modulus, the adhesion force of the SnC-derived sEVs is much higher than that of the non-SnC-derived sEVs. This is strong evidence that positively charged extra molecules (e.g., SASPs) are attached to the surfaces of SnC-derived sEVs. These molecules could make SnC-derived sEVs more rigid, whereby the DMT moduli of such vesicle composites could be altered.[2-5]
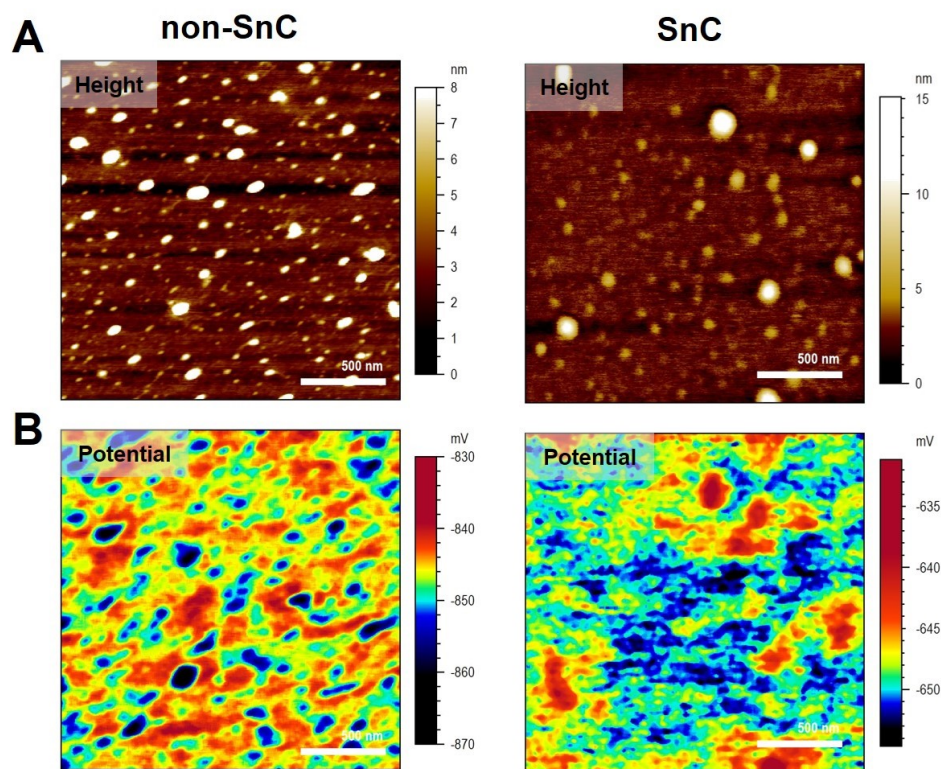
**Figure S7.** (A) Topographical AFM mapping and (B) nanoelectrical property mapping of non-SnC-derived sEVs (left) and SnC-derived sEVs (right). Scan size is 4 μm × 4 μm at 512 × 512 pixels.
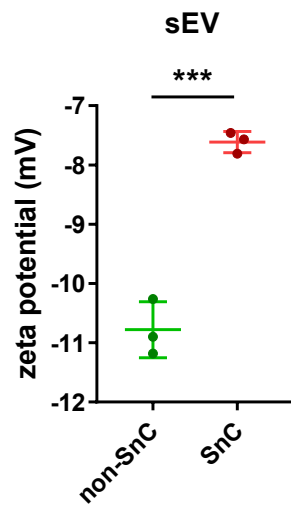
**Figure S8.** Zeta potential data of sEVs isolated from non-SnCs and SnCs (n = 3 per group). All values are mean ± S.D. ***$p < 0.001$. A two-tailed unpaired t-test was used for statistical analysis.
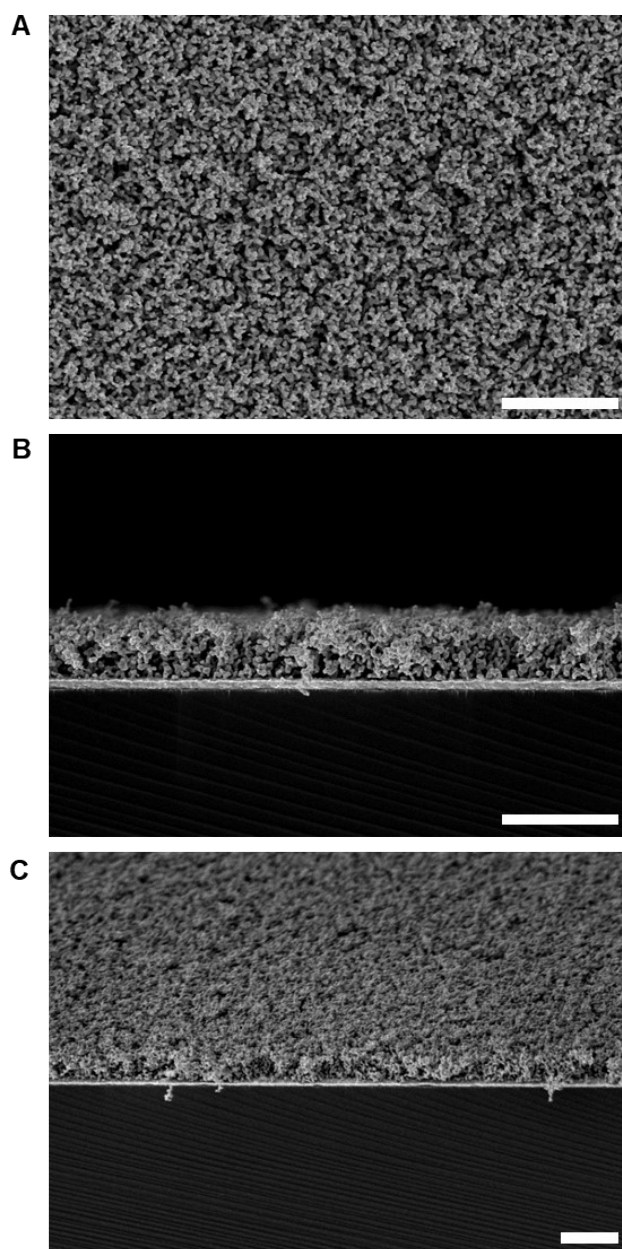
**Figure S9.** Scanning electron microscopic images of silver nanoforest (SNF) substrate. (A) Top view, (B) side view, and (C) 45°-tilted view. Scale bars represent 2.5 μm. The sizes of the single nanoparticles were approximately 50–100 nm, and the thickness of the nanoporous structure composed of silver nanoparticles was approximately 1 μm. The Raman signals from the samples dropped onto the SNF substrate were thought to be amplified by these stacked silver nanostructures.
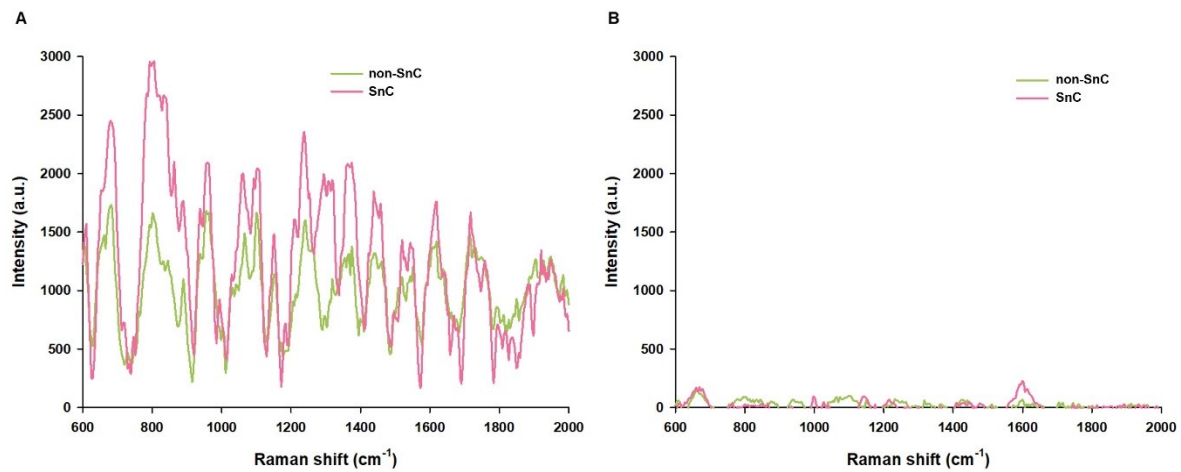
**Figure S10. Comparison between sEVs and cell-cultured media.** Raman spectra for (A) non-SnC and SnC-derived sEVs and (B) the non-SnC and SnC-cultured media after baseline correction.
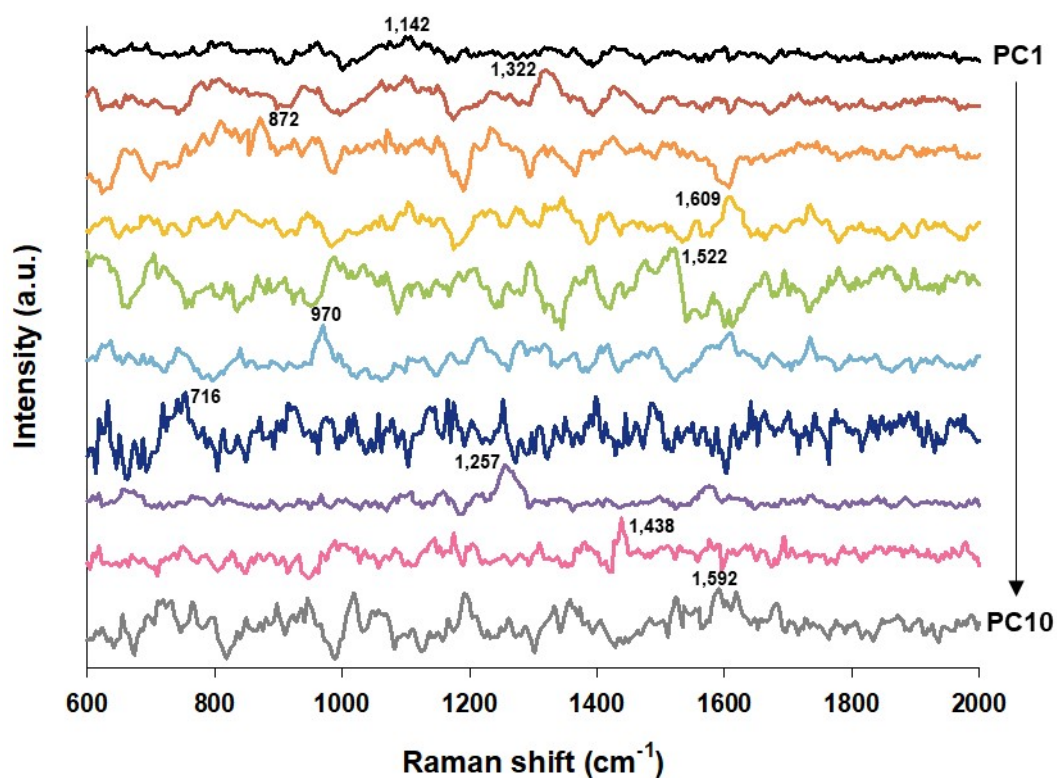
**Figure S11. The first 10 principal component (PC) loading vectors.** PC1 to PC10 were calculated using entire sEVs dataset (100 for each group). Projecting the Raman spectra onto these 10 principal component axes yields 10 scores. As described in the Methods section, the first 10 PC scores for each sEV were subjected to hierarchical clustering analysis using Ward's method to create linkages based on Euclidean pairwise distances. The first 5 PCs were the most significant different peaks between non-SnC- and SnC-derived sEVs. Spectra from the first 5 PCs were 872, 1,142, 1,322, 1,522, and 1,609 $cm^{-1}$ as shown in Figure 5A from the main text.

**A**

non-SnC    SnC

Intensity (a.u.)

600  800  1000  1200  1400  1600  1800  2000

Raman shift (cm⁻¹)

**B**

● non-SnC    ■ SnC

PC3
-0.5
-0.6
-0.7
-0.8
-0.9
-1.0
-1.1
-1.2

0.35  0.30  0.25  0.20

PC2

-0.3
-0.4
-0.5
-0.6
-0.7
-0.8
-0.9
-1.0

PC1

**C**

Intensity (a.u.)

140
120
100
80
60
40
20
0

non-SnC    SnC

**D**

Intensity ratio

1.2
1.0
0.8
0.6
0.4
0.2
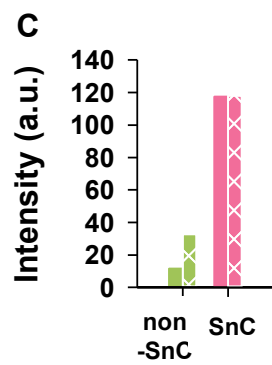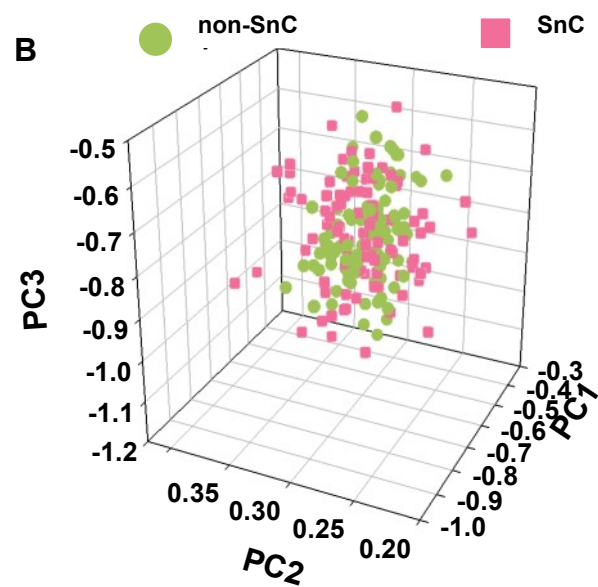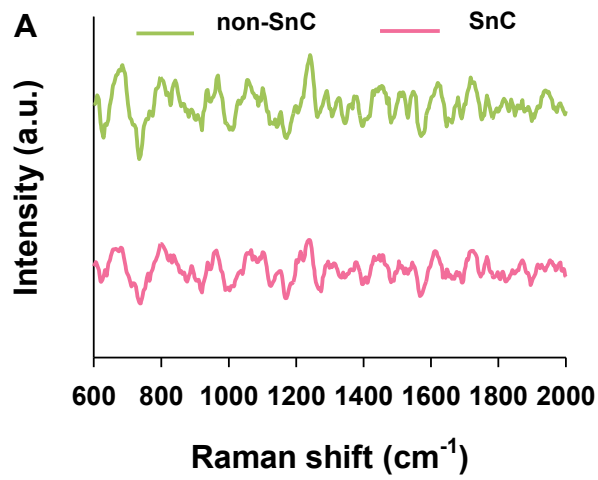
non-SnC    SnC
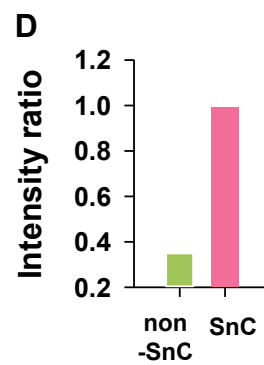
**Figure S12. Further analysis of lEVs (microvesicles) using Raman spectroscopy.** (A) Raman spectra of lEVs from non-SnCs and SnCs. Colored boxes represent characteristic Raman peaks related to amino acids. (B) 3D-PCA scores plot of each single Raman dataset for the first, second, and third principal components (PCs). (C) Raman intensities of characteristic peaks for (+) and (−) charged amino acids. Non-patterned and patterned bar plots represent the summation of Raman intensities at the characteristic peaks of (+) and (−) charged amino acids, respectively. (D) Raman intensity ratios of (+) and (−) charged amino acids using each value of summation of Raman intensities at the characteristic peaks for (+) and (−) charged amino acids.

**Supplementary Tables**

**Table S1.** Positions and descriptions of characteristic amino acids peak

| Raman shift (cm$^{-1}$) | Description |
|---|---|
| 716 | C–N (membrane phospholipids head)[6] |
| 783 | Symmetric breathing of tryptophan[7] |
| 872 | COOH deformation vibration of glutamic acid[8] |
| 970 | Lipids (phosphate monoester groups of phosphorylated proteins and nucleic acids)[9] |
| 1,044 | Symmetric stretching vibration of $v_3PO_4^{3-}$ for Proline[10] |
| 1,142 | $NH_3^+$ asymmetric rocking of lysine[11] |
| 1,183 | Cytosine, guanine, adenine[12] |
| 1,267 | Cytosine[13] |
| 1,322 | $NH_3^+$ asymmetric rocking of histidine[14] |
| 1,386 | C=O symmetric stretch/$CH_2$ deformation/NH in-plane deformation[15] |
| 1,438 | CH2 and CH3 deformation vibrations, cholesterol, fatty acid band[16] |
| 1,522 | $COO^-$ stretching vibration of aspartic acid[17] |
| 1,592 | G (DNA/RNA), CH deformation (proteins, and carbohydrates)[18] |
| 1,609 | $NH_3^+$ asymmetric bending of arginine[19] |

**Table S2.** pI value and charge at pH 7.4 of proteins enriched in SnC-derived sEVs, based on proteomics data

| Gene | Protein descriptions | pI value | charge at pH 7.4 | log2 FC (SnC/non-SnC) | q value |
|------|---------------------|----------|------------------|----------------------|---------|
| PSMB6 | Proteasome subunit beta type-6 | 4.91 | − | 2.43 | 5.65E-07 |
| PCOLCE | Procollagen C-endopeptidase enhancer 1 | 7.55 | + | 2.43 | 1.37E-04 |
| **IGFBP7** | **Insulin-like growth factor-binding protein 7** | **8.06** | + | **2.31** | **9.33E-09** |
| YBX1 | Nuclease-sensitive element-binding protein 1 | 9.87 | + | 2.30 | 1.77E-02 |
| **GREM1** | **Gremlin-1** | **9.55** | + | **2.30** | **2.28E-02** |
| GREM2 | Gremlin-2 | 9.3 | + | 2.30 | 2.28E-02 |
| LAMA4 | Laminin subunit alpha-4 | 5.84 | − | 2.29 | 1.87E-43 |
| COL5A2 | Collagen alpha-2(V) chain | 6.29 | − | 2.27 | 3.02E-08 |
| MKI67 | Marker of Ki-67 | 9.49 | + | 2.26 | 4.80E-02 |
| CKAP5 | Cytoskeleton-associated protein 5 | 7.95 | + | 2.12 | 1.07E-02 |
| NID1 | Nidogen-1 | 5.05 | − | 2.09 | 2.69E-21 |
| C1R | Complement C1r subcomponent | 5.76 | − | 2.08 | 3.85E-15 |
| APOM | Apolipoprotein M | 5.66 | − | 2.08 | 2.21E-02 |
| TAOK2 | Serine/threonine-protein kinase TAO2 | 6.84 | − | 2.03 | 5.05E-03 |
| TGFBI | Transforming growth factor-beta-induced protein ig-h3 | 7.37 | − | 1.99 | 5.94E-35 |
| LTA4H | Leukotriene A-4 hydrolase | 5.8 | − | 1.95 | 3.83E-02 |
| FBN1 | Fibrillin-1 | 4.74 | − | 1.94 | 2.33E-15 |
| FBLN1 | Fibulin-1 | 5.03 | − | 1.93 | 3.22E-14 |
| ESYT1 | Extended synaptotagmin-1 | 5.57 | − | 1.92 | 8.90E-03 |
| COL3A1 | Collagen alpha-1(III) chain | 9.36 | + | 1.91 | 2.35E-08 |
| DCN | Decorin | 8.76 | + | 1.89 | 2.78E-10 |
| LAMB1 | Laminin subunit beta-1 | 4.81 | − | 1.87 | 1.66E-50 |
| ANP32B | Acidic leucine-rich nuclear phosphoprotein 32 family member B | 3.93 | − | 1.87 | 4.64E-02 |
| TIMP2 | Metalloproteinase inhibitor 2 | 6.48 | − | 1.87 | 1.73E-05 |
| FN1 | Fibronectin | 5.25 | − | 1.82 | 1.66E-109 |
| **ANXA2** | **Annexin A2** | **7.56** | + | **1.82** | **3.63E-16** |

* Significantly changed proteins (q value < 0.05, log2(SnC/non-SnC) > 1.5), sorted by highest fold-change [20]

# REFERENCES

1. J. Rodriguez, A. Rico, E. Otero and W. M. Rainforth, *Acta Materialia*, 2009, **57**, 3148-3156.
2. V. Y. Bairamukov, A. S. Bukatin, R. A. Kamyshinsky, V. S. Burdakov, E. B. Pichkur, T. A. Shtam and M. N. Starodubtseva, *Biochimica et Biophysica Acta (BBA) - General Subjects*, 2022, **1866**, 130139.
3. M. Haro, V. Singh, S. Steinhauer, E. Toulkeridou, P. Grammatikopoulos and M. Sowwan, *Advanced Science*, 2017, **4**, 1700180.
4. M. Criado, E. Rebollar, A. Nogales, T. A. Ezquerra, F. Boulmedais, C. Mijangos and R. Hernández, *Biomacromolecules*, 2017, **18**, 169-177.
5. J. S. Gonzalez, C. Mijangos and R. Hernandez, *Polymers*, 2019, **11**, 702.
6. N. Stone, C. Kendall, J. Smith, P. Crow and H. Barr, *Faraday Discussions*, 2004, **126**, 141-157.
7. Z. Huang, A. McWilliams, H. Lui, D. I. McLean, S. Lam and H. Zeng, *International Journal of Cancer*, 2003, **107**, 1047-1052.
8. G. Zhu, X. Zhu, Q. Fan and X. Wan, *Spectrochimica Acta Part A: Molecular and Biomolecular Spectroscopy*, 2011, **78**, 1187-1195.
9. R. K. Dukor, in *Handbook of Vibrational Spectroscopy*, 2006.
10. C. J. Frank, R. L. McCreery and D. C. B. Redd, *Analytical Chemistry*, 1995, **67**, 777-783.
11. B. Hernández, F. Pflüger, N. Derbel, J. De Coninck and M. Ghomi, *The Journal of Physical Chemistry B*, 2010, **114**, 1077-1088.
12. P. Wang, W. Zhang, O. Liang, M. Pantoja, J. Katzer, T. Schroeder and Y.-H. Xie, *ACS Nano*, 2012, **6**, 6244-6249.
13. S. Yue, J. Li, S.-Y. Lee, Hyeon J. Lee, T. Shao, B. Song, L. Cheng, Timothy A. Masterson, X. Liu, Timothy L. Ratliff and J.-X. Cheng, *Cell Metabolism*, 2014, **19**, 393-406.
14. F. Pflüger, B. Hernández and M. Ghomi, *The Journal of Physical Chemistry B*, 2010, **114**, 9072-9083.
15. S. Farquharson, C. Shende, F. E. Inscore, P. Maksymiuk and A. Gift, *Journal of Raman Spectroscopy*, 2005, **36**, 208-212.
16. W. Schneider, T. Bortfeld and W. Schlegel, *Physics in Medicine and Biology*, 2000, **45**, 459-478.
17. J. T. L. Navarrete, V. Hernández and F. J. Ramírez, *Biopolymers*, 1994, **34**, 1065-1077.
18. N. Dieter, *Proc.SPIE*, 1998, **3257**.
19. L.-Y. Jiang, X.-S. Li, A.-J. Wang, H. Huang and J.-J. Feng, *Journal of Colloid and Interface Science*, 2017, **498**, 128-135.
20. N. Basisty, A. Kale, O. H. Jeon, C. Kuehnemann, T. Payne, C. Rao, A. Holtz, S. Shah, V. Sharma, L. Ferrucci, J. Campisi and B. Schilling, *PLoS Biol*, 2020, **18**, e3000599.